NANO LETTERS

Letter

pubs.acs.org/NanoLett

Gold Catalyzed Nickel Disilicide Formation: A New Solid–Liquid–Solid Phase Growth Mechanism

Wei Tang,*[,†,‡] S. Tom Picraux,[‡] Jian Yu Huang,[∥] Xiaohua Liu,[∥] K. N. Tu,[†] and Shadi A. Dayeh*[,‡,§]

[†]Department of Materials Science and Engineering, University of California, Los Angeles, Los Angeles, California 90024, United States

[‡]Center for Integrated Nanotechnologies, Los Alamos National Laboratory, Los Alamos, New Mexico, 87545, United States

[§]Department of Electrical and Computer Engineering, University of California, San Diego, La Jolla, California, 92093, United States

[∥]Center for Integrated Nanotechnologies, Sandia National Laboratories, Albuquerque, New Mexico 87123, United States

Supporting Information

ABSTRACT: The vapor–liquid–solid (VLS) mechanism is the predominate growth mechanism for semiconductor nanowires (NWs). We report here a new solid–liquid–solid (SLS) growth mechanism of a silicide phase in Si NWs using in situ transmission electron microcopy (TEM). The new SLS mechanism is analogous to the VLS one in relying on a liquid-mediating growth seed, but it is fundamentally different in terms of nucleation and mass transport. In SLS growth of Ni disilicide, the Ni atoms are supplied from remote Ni particles by interstitial diffusion through a Si NW to the pre-existing Au–Si liquid alloy drop at the tip of the NW. Upon supersaturation of both Ni and Si in Au, an octahedral nucleus of Ni disilicide ($NiSi_2$) forms at the center of the Au liquid alloy, which thereafter sweeps through the Si NW and transforms Si into $NiSi_2$. The dissolution of Si by the Au alloy liquid mediating layer proceeds with contact angle oscillation at the triple point where Si, oxide of Si, and the Au alloy meet, whereas $NiSi_2$ is grown from the liquid mediating layer in an atomic stepwise manner. By using in situ quenching experiments, we are able to measure the solubility of Ni and Si in the Au–Ni–Si ternary alloy. The Au-catalyzed mechanism can lower the formation temperature of $NiSi_2$ by 100 °C compared with an all solid state reaction.

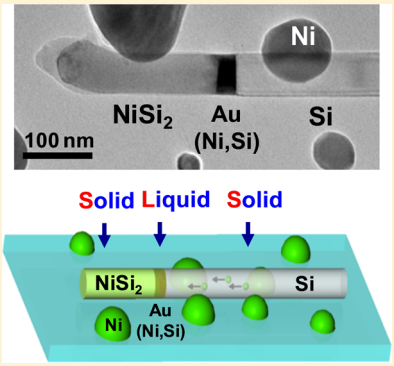

KEYWORDS: *Nickel silicide, silicon nanowire, in situ TEM, ternary alloy, liquid mediating, homogeneous nucleation*

The vapor–liquid–solid (VLS) growth mechanism has been extensively used to grow one-dimensional (1D) Si, Ge, III–V semiconductor nanowires (NWs) and their heterostructures. Such 1D NWs have demonstrated potential applications in nanoscale electronic[1−3] and opto-electronic devices.[4−7] In the VLS growth, Au is frequently used as the growth seed. It satisfies a number of critical requirements for growing 1D NWs, such as being a catalyst for gas precursor decomposition at its surface, which has a high accommodation coefficient for impinging adatoms. This enables the formation of a supersaturated liquid that can precipitate a 1D crystal through layer-by-layer crystallization at a low energy interface.[8] The fascinating science of this growth mechanism has been the subject of many decades of research, and it continues to be an area of increased attention for demonstrating for instance heterostructured NWs that may not be possible without the VLS approach.[9,10] In effect, the VLS mechanism helps reduce the growth temperature of a single crystalline Si solid phase, to temperatures that are very close to the Au–Si eutectic temperature (363 °C). In comparison, to grow defect-free single crystalline Si directly from gas phase (e.g., MBE growth), the substrate has to be heated above 800 °C in order to maintain high diffusivity of Si atoms on the surface of the epitaxial layer.[11] In contrast to VLS growth of semiconductors, metallic NWs have been generally synthesized by a solution–liquid–solid mechanism analogous to the VLS,[12] template-assisted approach,[13] or by direct and purely solid-state reactions between metal and semiconductor NWs.[14]

Here, we establish a new growth mechanism for metallic NWs by the solid–liquid–solid (SLS) mechanism. Through detailed in situ transmission electron microscopy (TEM) studies on Au-catalyzed $NiSi_2$ formation within Si NWs, we demonstrate the concept of catalytic liquid mediated growth (similar to VLS) of a solid metallic $NiSi_2$ NW. In such reaction, reactant species are delivered through solid phase diffusion, in contrast to the gas phase transport in the VLS growth mechanism. Despite the analogy in using a liquid phase to mediate a layer-by-layer growth, the nucleation and growth of the $NiSi_2$ phase are dramatically different from those in VLS. Our systematic in situ real time monitoring of these processes shed light on the new and fascinating aspects of this growth mechanism. Further, we quantitatively extracted the thermodynamic solubility limit in the Au–Ni–Si ternary alloy, which is

Received: August 27, 2013
Revised: November 20, 2013
Published: November 25, 2013

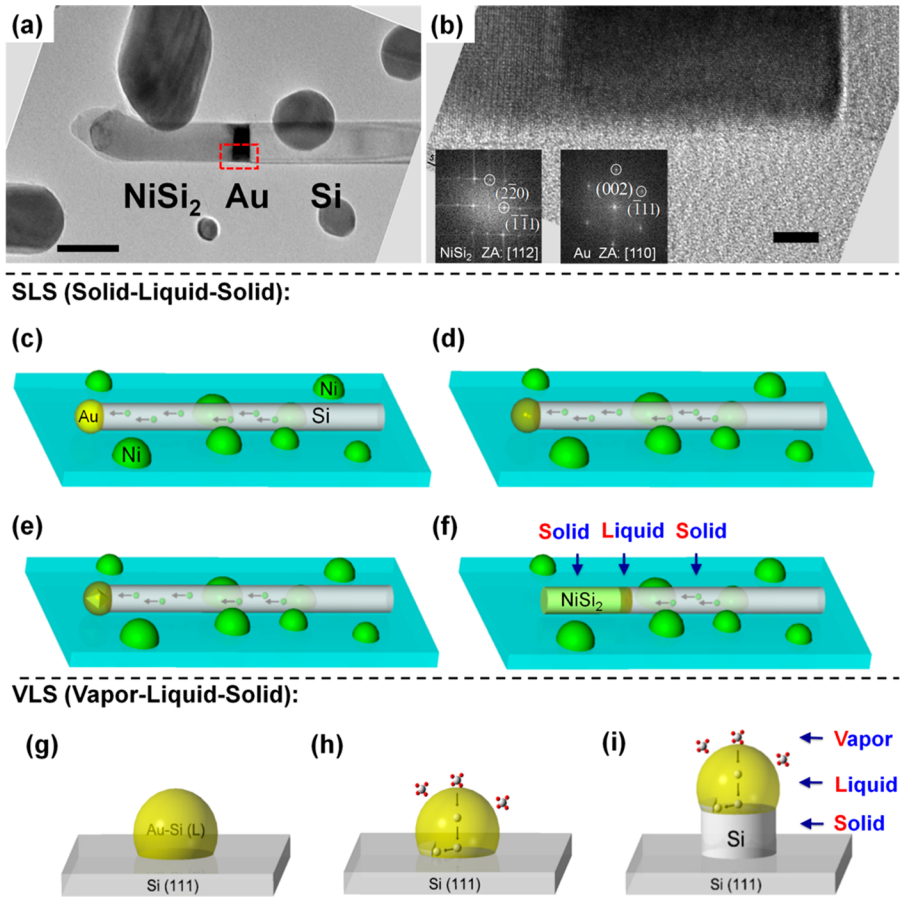

Figure 1. (a) TEM bright field image showing $NiSi_2$ forms from the tip of the nanowire with a Au alloy layer moving toward the opposite end. The scale bar is 100 nm. (b) HRTEM image of the area around Au. The reaction front is a $NiSi_2$ (111) plane that maintains a (111) interface with the solidified Au as demonstrated in the inset FFT patterns. The scale bar is 5 nm. *SLS growth process*: (c) Ni interstitial diffusion through a Si medium (NW) and accumulation in the Au−Si eutectic alloy. (d) Formation of a liquid Au−Ni−Si ternary alloy at the Si NW tip. (e) Nucleation and growth of a single octahedral $NiSi_2$ crystallite inside the liquid ternary alloy. (f) Continuous dissolution of the Si NW by the eutectic ternary that moves down through the Si NW and concurrent growth of $NiSi_2$ on the other side of the eutectic in the steady state. *VLS growth process*: (g) Eutectic alloying between Au particle and Si substrate. (h) Introduction of reactant species by gas phase followed by supersaturation and nucleation of a Si step at the edge of a Au−Si eutectic alloy. (i) Continuous growth of Si NW in the steady state.

used as a contact material for III−V semiconductors,[15] and is also relevant to Ni/Au contacts on Si.[16]

Our experimental platform utilizes a 30 nm silicon nitride TEM membrane as the substrate (transparent to the electron beam) with Ni nanoparticles (NPs), which were formed by annealing a predeposited thin layer of Ni (6 nm) at 650 °C in forming gas for 2 min. Si NWs were dispersed on the membrane to make random contact with the Ni NPs. The diameters of Ni NPs and Si NWs were generally around 100 nm. The whole substrate was then mounted on a Gatan 628 single tilt heating stage and transferred into the TEM (FEI Tecnai F30, base vacuum 8×10^{-8} Torr) chamber. The temperature of the heater was measured by a thermocouple and can be manually controlled by an external current source. Unless otherwise specified, the temperature of the heating stage was kept at 700 °C as the isothermal treatment to trigger and sustain the reaction between Ni and Si. TEM images were continuously captured in real time and compiled into videos from which we composed the figures presented in this paper.

Our first striking observation was that, upon annealing of the samples discussed above at 700 °C for 50 min, a $NiSi_2$ silicide growth segment initiates from the tip of the Si NW with concurrent movement of the Au alloy seed toward the other end (base) of the NW (Figure 1a and f), in which the liquid Au alloy is sandwiched between the two solid phases of Si and silicide. This is in contrast to commonly known silicide formation mechanisms both in bulk[17,18] and at the nanoscale,[19,20] where Au was not involved. A high-resolution (HR) TEM image (Figure 1b) shows that the nickel silicide phase is $NiSi_2$, and the (111) plane of $NiSi_2$ is its growth front. Further systematic in situ studies have revealed details on the atomic-scale reactions during this new silicide growth process. We will first provide a general perspective on the processes involved in this growth and follow by experimental verification of these processes.

We attribute the Au-catalyzed $NiSi_2$ formation to a SLS growth mechanism. In the SLS growth of $NiSi_2$, Ni atoms dissolve from Ni NPs in contact with the Si NW into the NW and diffuse interstitially to and accumulate at the Au tip of the NW (Figure 1c). Upon supersaturation of both Si (available from the Si NW itself) and Ni in the Au−Ni−Si ternary liquid alloy (Figure 1d), a single solid octahedral shape of $NiSi_2$ crystallite nucleates and grows in the liquid alloy (Figure 1e). With continuous Ni supply through diffusion in the Si NW to the Au alloy and concurrent dissolution of Si layers at the alloy−Si interface, the $NiSi_2$ precipitate grows at the other end

dx.doi.org/10.1021/nl4032023 | *Nano Lett.* 2013, 13, 6009−6015

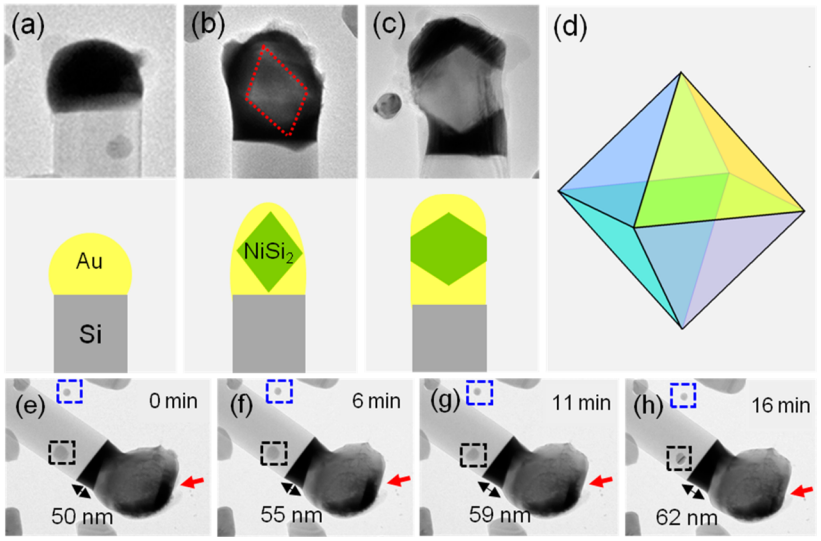

Figure 2. (a) TEM image of the liquid Au−Si alloy which acts as a Ni sink. (b) Emerging $NiSi_2$ octahedral crystallite inside the Au liquid ternary alloy. (c) Expansion of the $NiSi_2$ crystallite to the boundaries of the Si NW and subsequent separation of the liquid ternary on opposite sides of the crystallite. (d) Schematic of an octahedral nucleus bounded by eight {111} facets. (e−h) In situ TEM snapshots showing (1) gradual reduction of the Au volume at the Si NW tip as indicated by red arrows, (2) expansion of the Au liquid mediating layer in length, as marked by double-headed arrows, (3) shrinkage of the Ni particle volume that is in contact with the Si NW, which is marked by black dashed boxes, and (4) no size change for the Ni particle not in contact with Si NW, which is marked by blue dashed boxes.

of the Au alloy in the steady state (Figure 1f). An alternative Ni diffusion path may be considered along the surface of the Si native oxide. However, previous ripening experiments showed that Ni surface diffusivity on the Si native oxide is insignificant at temperatures that are as high as 800 °C.[20] Moreover, it was shown that replacing the Si native oxide by other surface coatings such as Al_2O_3 and carbon did not affect the Ni silicide growth rate in Si NWs.[21] Therefore, the surface diffusion mechanism can be ruled out. On the other hand, the Ni interstitial diffusivity in Si is on the order of 10^{-12} m^2/s at 700 °C,[22] so Ni atoms can diffuse over several micrometers in a few seconds, and such a diffusion process is hence sufficient to support the SLS $NiSi_2$ growth.

Detailed understanding of this phase formation requires a complete knowledge of the Au−Ni−Si ternary phase diagram, which is still lacking in the literature. However, we can derive qualitative information from their binary phase diagrams. In the binary Au−Ni system, their solid phases are consolute above 816 °C and also appreciably soluble to each other at lower temperature, which implies a low enthalpy term for their solid solution and good compatibility between Ni and Au atoms. In contrast, Ni solubility in Si is negligible ($\sim 10^{15} cm^{-3}$)[23] even at 700 °C, implying a high enthalpy term. Therefore, Au acts as a getter/sink of Ni in the Si NW and tends to react with the incoming Ni atoms supplied from remote Ni sources. Since Si is abundant from the Si NW itself, growth of the $NiSi_2$ phase is therefore limited by the supply of Ni atoms. At the Ni/Au interface, the Au liquid alloy absorbs incoming Ni so that the latter is depleted in the part of Si NW close to Ni/Au interface, which creates a Ni concentration gradient in the Si NW and maintains the continuous delivery of Ni atoms (see Figure S1 in the Supporting Information for schematics of the chemical potential and Ni concentration profiles along the axial direction of the NW). Although the Ni concentration increases when it enters Au, the chemical potential drops due to a reduced enthalpy term described above.

To compare the SLS and the VLS growth mechanisms, we recall that the latter starts with a Au particle, which forms a liquid alloy with Si when the Si substrate is heated above the Au−Si eutectic temperature (363 °C, Figure 1g). Additional Si atoms are introduced from the vapor phase (e.g., SiH_4) and supersaturate in the Au−Si alloy. The solid Si phase nucleates at the edge of the liquid−solid interface (Figure 1h) and continues to grow epitaxially with continuous supply of SiH_4 (Figure 1i). We note that both VLS and SLS are liquid-mediated, and both precipitate out solid phases. To enable successful liquid mediated solid phase growth, the eutectic melt should have a lower temperature than the melting point of the solid phase that is intended to form. In VLS growth of Si NW, the Si melting temperature is 1414 °C, and the Au−Si eutectic temperature is 363 °C; while in SLS growth of $NiSi_2$, the melting point of $NiSi_2$ is 997 °C, and the Au−Ni−Si eutectic melt temperature should be below 700 °C, since 700 °C is our annealing temperature and the Au-rich segment does not show any characteristic diffraction spots originating from a crystal at various tilt angles indicating a molten alloy. The difference between VLS and SLS growth resides in the nucleus formation and the mass transport mechanism of source atoms. These two aspects will be discussed in detail in the following experiments.

By using the in situ TEM technique, we are able to observe dynamically the events of nucleation and early stage growth of the $NiSi_2$ phase from the Au liquid alloy. Initially, upon heating, the Au tip forms a eutectic liquid with Si NWs and continues to accept incoming Ni atoms (Figure 2a). When both Ni and Si reach supersaturation in the Au eutectic liquid, a $NiSi_2$ octahedral shape nucleus (or more accurately crystallite) emerges in the middle of the liquid Au (Figure 2b). It is a nanoscale verification of crystal growth following the Wulff plot; the octahedral facets have the slowest growth rate. The liquid state of the Au ternary alloy was confirmed by examining a large number of Au tips at different stages of incubation or nucleation, and no signs of solidification (e.g., surface faceting or diffraction contrast) of the Au ternary alloy were observed.

dx.doi.org/10.1021/nl4032023 | Nano Lett. 2013, 13, 6009−6015

The $NiSi_2$ crystal continues to grow while retaining its octahedral shape until its size reaches the diameter of the NW. At this point, the originally suspended $NiSi_2$ octahedron is anchored at the boundary edges of the Si NW (Figure 2c) and consequently splits the Au liquid into two parts (the part at the tip and the liquid mediating layer at the other side of the $NiSi_2$ crystal). The part of Au at the tip gradually migrates on the $NiSi_2$ surface to the other side of the Au mediating layer (Figure 2e–h), as indicated by the increase of the Au mediating layer volume and the gradual reduction of the Au volume at the tip end. It is worth noting that the Ni particle highlighted by a dashed black box (in Figure 2e–h) gradually shrinks over the time period of our observation, which substantiates the fact that Ni is indeed diffusing toward the ternary tip and that the particular Ni particle is one of the Ni supply sources for the silicide growth. In contrast, the Ni particle on the silicon nitride membrane highlighted by blue dashed box does not show any size evolution with time, and this rules out the possibility that the Ni supply that is needed for $NiSi_2$ formation occurs by surface diffusion on the nitride membrane.

An interesting aspect of the SLS growth is that the $NiSi_2$ crystallite nucleates homogeneously from the liquid. In general, it is well-known that homogeneous nucleation is rare because it requires a very high supersaturation to overcome the nucleation barrier.[24] In reality, phase transformation is usually initiated by heterogeneous nucleation. We recently reported an in situ TEM study of preferred heterogeneous nucleation of Ni silicide at Si crystalline boundaries.[25] VLS growth of Si NWs is another example of heterogeneous nucleation, where it has been experimentally demonstrated that the Si crystal nucleates at the surface of the Au–Si eutectic liquid.[26] However, in contrast, in our Au catalyzed $NiSi_2$ growth, an octahedrally shaped nucleus (bounded by {111} facets) emerges in the middle of the Au ternary alloy. This octahedral shape is believed to be the Wulff shape of a $NiSi_2$ crystal, and similar octahedral precipitates have been observed in the reaction between amorphous silicon and implanted Ni.[27,28] Actually, there are two possible heterogeneous nucleation interfaces: (1) the interface between the Au ternary alloy and the Si NW and (2) the interface between the Au ternary alloy and its thin encapsulating SiO_2 layer [as-grown Si NW gold tips are usually encapsulated by a thin oxide layer (Figure S2, Supporting Information), which may be due to Au-catalyzed low temperature SiO_2 formation,[29,30] post growth oxidation, or residual Si at the surface of the frozen Au tip]. As previously found, Ni is the dominant diffusion species in $NiSi_2$.[31] Therefore, heterogeneous nucleation of $NiSi_2$ at the interface of the alloy/Si NW is not likely. This is because the $NiSi_2$ layer forming in this way will block and eventually rule out the accessibility of the Si NW to the ternary eutectic Au alloy and consequently cut off the Si atom supply for the silicidation reaction, because the diffusion of Si in $NiSi_2$ is slow. The absence of silicide nucleation at the alloy/SiO_2 interface implies that the $NiSi_2/SiO_2$ interface has high energy, and therefore such an interface is not a favorable heterogeneous nucleation site. Although TEM images are 2D projections, we examined a large number of $NiSi_2$ crystallite in the Au tip at different tilt angles and different stages of growth (additional examples are shown in Figure S5), and we found no signatures of heterogeneous nucleation (i.e., $NiSi_2$ growth initiating from certain peripheral boundaries). This observation is consistent with previous findings,[32] which showed that stepwise growth of nickel silicide within a Si NW proceeds through the repeating 2D homogeneous nucleation, where the high-energy oxide/silicide interface hinders a heterogeneous nucleation.

The in situ TEM technique provides us with a unique opportunity to study quantitatively the thermodynamic properties of the Au–Ni–Si ternary system. We measured Ni and Si solute concentrations in the ternary Au–Ni–Si alloy at 700 °C during the steady state growth of $NiSi_2$ by a quenching experiment. As previously discussed, there is no ternary phase diagram information available for the Au–Ni–Si system. By quenching the mediating ternary Au–Ni–Si liquid alloy from 700 °C to room temperature and by measuring the volume of Si and $NiSi_2$ precipitated out at both ends of the Au alloy, we can provide quantitative information to the Au–Ni–Si ternary phase diagram. We chose a quench rate (~2 °C/s) that is slow enough to ensure that all of the Si (and Ni) are ejected from the Au alloy but is still relatively fast when compared to the $NiSi_2$ growth rate (0.05–0.1 nm/s), which therefore provides a robust method to measure the Si composition in the Au–Ni–Si ternary system. Figure 3a–b shows a comparison of the volume

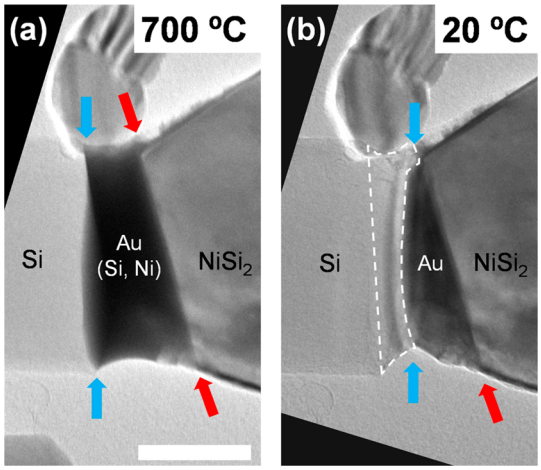

Figure 3. Au mediating layer before (a) and after (b) quenching from 700 °C. The Au/$NiSi_2$ interface indicated by red arrow does not move, while the Si/Au interface marked by blue arrow contracts with Si precipitated out from Au (highlighted by white dashed enclosure). The scale bar is 50 nm.

of the Au mediating layer before and after quenching from 700 °C. There is no observable $NiSi_2$ precipitated out from the Au mediating layer, which implies that the Ni solute saturation concentration required for $NiSi_2$ growth is low (<1%). This is also consistent with previous discussions that Ni is the limiting source in $NiSi_2$ growth. Due to the very high diffusivity of Ni at 700 °C, the Ni supply is likely to be limited by the process of Ni dissolution into the Si NWs through the native oxide layer, which is known to be a slow process. By calculating the amount of Si precipitated out and the volume of remaining Au at room temperature (see details in the Supporting Information, Figure S3), the Si/Au atomic ratio at 700 °C in the Au–Ni–Si ternary alloy was determined to be 0.54:1. According to the Si–Au binary phase diagram, the solubility limit of Si in equilibrium Au–Si liquid in contact with Si translates to a Si/Au atomic ratio of 2.2:1 in such a saturated liquid alloy (the liquidus line to the Si side at 700 °C). This observation implies that, in the Au–Ni–Si ternary system, the presence of a small amount of Ni can reduce the solubility of Si in Au approximately by a factor of 4, because of the preferable precipitation of $NiSi_2$ rather than elemental Si. On the other hand, this experiment

dx.doi.org/10.1021/nl4032023 | Nano Lett. 2013, 13, 6009–6015

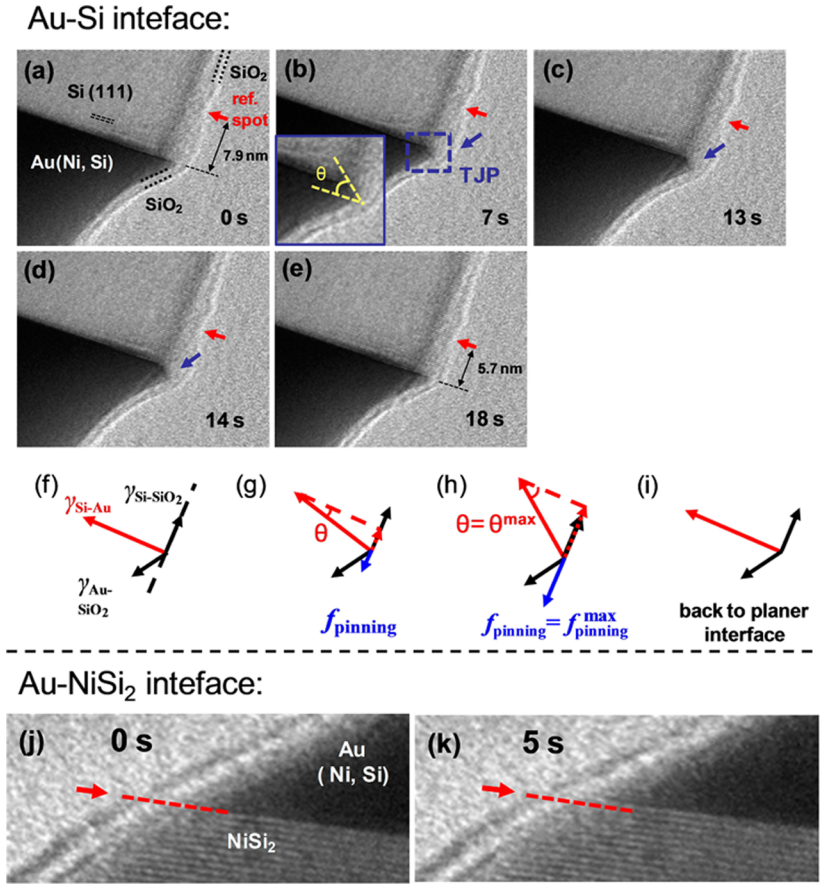

Figure 4. *Au−Si interface*: (a−e) in situ TEM snapshots showing one cycle of contact angle oscillation at the triple junction point. The red arrow indicates a reference spot on the NW surface. The blue arrow indicates curvature develops at the triple junction point. (f−i) Force analysis of the mechanism of contact angle oscillation at the triple junction point. *Au−NiSi$_2$ interface*: (j−k) growth of a single $NiSi_2$ (111) layer.

demonstrates that the slow $NiSi_2$ growth proceeds with small supersaturation of Ni in the ternary alloy, while Si remains near its equilibrium concentration in the Au−Ni−Si alloy. These observations demonstrate that the in situ TEM heating and quenching technique can be very useful in extracting phase diagram information in complex systems not attainable by conventional methods.[33]

One of the fascinating aspects of this new $NiSi_2$ SLS growth mechanism is the concurrent dissolution of Si at one interface with the Au ternary alloy and crystallization of $NiSi_2$ on the opposite interface of the ternary alloy. By closely monitoring the Au/Si interface movement, we observed a peculiar contact angle oscillation at the triple phase boundary where the Au ternary alloy dissolves the Si (111) planes progressively. In contrast, growth of $NiSi_2$ at the $NiSi_2$/Au alloy interface occurs in a well-defined stepwise manner. We will first discuss the moving Au/Si interface and then briefly discuss the movement of the $NiSi_2$/Au interface.

Figure 4a−e shows a series of TEM snapshots of Au/Si interface movement. We define the periphery where Si/Au/native-SiO_2 meet as the triple junction point (TJP, shown in Figure 4b). When the Si concentration in the Au liquid alloy is below its saturation point, the Au is able to dissolve Si from the NW. The interface, however, does not remain planar while it is moving. Au tends to dissolve Si at the center part of the NW first, while the movement of TJP is retarded with respect to the dissolution front. As a result, curvature at TJP develops and continues to increase as the Au further dissolves Si at the center. We use the contact angle θ illustrated in the inset of Figure 4b as a measure of the curvature change. The TJP does not move forward until θ reaches a certain threshold value (Figure 4d), and the Au/Si interface becomes flat again after TJP movement (Figure 4e). The process described above constitutes one cycle of contact angle oscillation during which 7 layers of Si (111) planes are dissolved (see Video 1 in the Supporting Information for multiple cycles of this process).

The contact angle oscillation behavior can be understood by analyzing the force balance at the TJP. Figure 4f shows surface/interface tension forces at the TJP when the Au/Si interface is flat. The force component along the dashed line direction should be balanced. When the contact angle θ increases, there is an additional force component of the Au/Si tension that projects along the dashed line direction. A pinning force appears to balance this additional force component (Figure 4g). The pinning force behaves like a macroscopic static friction force, and it may originate from microscopic heterogeneity at the Si/SiO_2 interface.[34] When θ increases, the force component along the dashed line direction increases, and the pinning force increases correspondingly until it reaches the maximum pinning force $f_{\text{pinning}}^{\max}$ (corresponding contact angle $\theta^{\max}$) that can be exerted by the native oxide shell (Figure 4h). After that, TJP movement can no longer be constrained, and the interface becomes flat again (Figure 4i). This contact angle oscillation can also be understood from the viewpoint of interfacial energetics. As the TJP moves, the Si/SiO_2 interface is replaced by a Au/SiO_2 interface. The Si/SiO_2 interface is well-known as

dx.doi.org/10.1021/nl4032023 | *Nano Lett.* 2013, 13, 6009−6015

a stable interface and has a low interfacial energy (γ = 0.7 J/m^2),[35] while the Au/SiO_2 interface has a higher interfacial energy (γ = 1.4 J/m^2).[36] Replacement of a low energy interface by a high energy interface is energetically unfavorable, so the movement of the TJP lags the forward moving Au ternary interface into the Si NW. Similar TJP-lagging phenomenon have been observed in other systems, such as the reaction between Co and Si NW, where the resultant $CoSi_2$ growth at the TJP lags behind the growth front at the NW center.[32]

In contrast to the contact angle oscillation behavior at the Si dissolution front, the growth front of $NiSi_2$ proceeds in a layer-by-layer fashion (see Video 2 in the Supporting Information). Figure 4j–k shows growth of one (111) atomic plane of $NiSi_2$. This result implies that the $f^{max}_{pinning}$ at the $NiSi_2$/SiO_2 interface may be low and θ^{max} is very small.

Without Au mediation, Ni and Si do not react directly until the temperature is raised to 800 °C in the type of sample we investigate. At 800 °C, $NiSi_2$ starts to nucleate homogeneously in the Si NW sample (Figure S4, Supporting Information), which implies that Au can catalyze the formation of $NiSi_2$ at a lower temperature (700 °C). Similar catalytic effects of Au are also suggested in Ni–Si thin film reactions.[37]

In summary, we report a new Au catalyzed SLS mechanism to synthesize metallic $NiSi_2$ nanowires with detailed studies by in situ TEM. Similar to VLS, the liquid phase lowers the nucleation barrier and facilitates the growth of a single crystal solid phase in SLS. Further, we demonstrate that a classical equilibrium Wulff shape of $NiSi_2$ crystallite homogeneously nucleates from the Au–Ni–Si ternary liquid, due to the unique geometry and interface energy combination of our SLS growth system. The thermodynamic dissolution limit of the Ni and Si solutes in the ternary liquid was quantitatively established by the in situ TEM quenching experiment. We monitored the dynamical movement of the liquid/solid interface and found that it may be hindered by the microheterogeneity at the NW/native oxide side wall. Our study suggests that a properly designed liquid-mediating process may provide an alternative integrated approach to synthesize metallic/semiconductor nanowire heterojunction devices and interconnects.

■ ASSOCIATED CONTENT

Supporting Information

Dynamical videos with Au/Si and $NiSi_2$/Au interface movement captured during the SLS growth steady state, schematics of Ni concentration and chemical potential during SLS growth steady state, calculation of the dissolved out Au and Si volumes during quenching experiment, and TEM image of $NiSi_2$ homogeneous nucleation at high temperature. This material is available free of charge via the Internet at http://pubs.acs.org.

■ AUTHOR INFORMATION

Notes

The authors declare no competing financial interest.

■ ACKNOWLEDGMENTS

This work was performed, in part, at the Center for Integrated Nanotechnologies (proposal no. C2011A1023), a U.S. Department of Energy, Office of Science User Facility. Los Alamos National Laboratory, an affirmative action equal opportunity employer, is operated by Los Alamos National Security, LLC, for the National Nuclear Security Administration of the U.S. Department of Energy under contract DE-AC52-06NA25396. We thank Professor Ning Wang from Hong Kong University of Science and Technology for training W.T. in TEM imaging. We thank Blythe Clark from Sandia National Laboratory for providing the in situ TEM heating stage and John Nogan for assistance in fabrication facilities at CINT. S.A.D. acknowledges support from a faculty start-up grant at UC San Diego.

■ REFERENCES

(1) Xiang, J.; Lu, W.; Hu, Y. J.; Wu, Y.; Yan, H.; Lieber, C. M. *Nature* **2006**, *441*, 489–493.
(2) Huang, Y.; Duan, X. F.; Cui, Y.; Lieber, C. M. *Nano Lett* **2002**, *2*, 101–104.
(3) Tang, W.; Dayeh, S. A.; Picraux, S. T.; Huang, J. Y.; Tu, K.-N. *Nano Lett* **2012**, *12*, 3979–3985.
(4) Johnson, J. C.; Choi, H. J.; Knutsen, K. P.; Schaller, R. D.; Yang, P. D.; Saykally, R. J. *Nat. Mater.* **2002**, *1*, 106–110.
(5) Qian, F.; Li, Y.; Gradecak, S.; Wang, D. L.; Barrelet, C. J.; Lieber, C. M. *Nano Lett.* **2004**, *4*, 1975–1979.
(6) Skold, N.; Karlsson, L. S.; Larsson, M. W.; Pistol, M. E.; Seifert, W.; Tragardh, J.; Samuelson, L. *Nano Lett.* **2005**, *5*, 1943–1947.
(7) Tian, B. Z.; Zheng, X. L.; Kempa, T. J.; Fang, Y.; Yu, N. F.; Yu, G. H.; Huang, J. L.; Lieber, C. M. *Nature* **2007**, *449*, 885–U8.
(8) Givargizov, E. I. *Highly anisotropic crystals*; D. Reidel Pub. Co.: Dordrecht, 1987.
(9) Dayeh, S. A.; Wang, J.; Li, N.; Huang, J. Y.; Gin, A. V.; Picraux, S. T. *Nano Lett.* **2011**, *11*, 4200–4206.
(10) Björk, M. T.; Ohlsson, B. J.; Sass, T.; Persson, A. I.; Thelander, C.; Magnusson, M. H.; Deppert, K.; Wallenberg, L. R.; Samuelson, L. *Nano Lett* **2002**, *2*, 87–89.
(11) Ota, Y. *Thin Solid Films* **1983**, *106*, 3–136.
(12) Trentler, T. J.; Hickman, K. M.; Goel, S. C.; Viano, A. M.; Gibbons, P. C.; Buhro, W. E. *Science* **1995**, *270*, 1791–1794.
(13) Sarkar, J.; Khan, G. G.; Basumallick, A. *Bull. Mater. Sci.* **2007**, *30*, 271–290.
(14) Wu, Y.; Xiang, J.; Yang, C.; Lu, W.; Lieber, C. M. *Nature* **2004**, *430*, 61–65.
(15) Yang, S. J.; Kang, T. W.; Kim, T. W.; Chung, K. S. *J. Mater. Res.* **2002**, *17*, 1019–1023.
(16) Kim, B.-H.; Cho, C.-H.; Park, S.-J.; Park, N.-M.; Sung, G. Y. *Appl. Phys. Lett.* **2006**, *89*, 063509–3.
(17) Tu, K. N.; Alessandrini, E. I.; Chu, W. K.; Krautle, H.; Mayer, J. W. *Jpn. J. Appl. Phys.* **1974**, 669–672.
(18) Gosele, U.; Tu, K. N. *J. Appl. Phys.* **1989**, *66*, 2619–2626.
(19) Lu, K. C.; Wu, W. W.; Wu, H. W.; Tanner, C. M.; Chang, J. P.; Chen, L. J.; Tu, K. N. *Nano Lett.* **2007**, *7*, 2389–2394.
(20) Wu, W. W.; Lu, K. C.; Wang, C. W.; Hsieh, H. Y.; Chen, S. Y.; Chou, Y. C.; Yu, S. Y.; Chen, L. J.; Tu, K. N. *Nano Lett.* **2010**, *10*, 3984–3989.
(21) Chen, Y.; Lin, Y.-C.; Zhong, X.; Cheng, H.-C.; Duan, X.; Huang, Y. *Nano Lett.* **2013**, *13*, 3703–3708.
(22) Spit, F. H. M.; Gupta, D.; Tu, K. N. *Phys. Rev. B* **1989**, *39*, 1255–1260.
(23) Istratov, A. A.; Zhang, P.; McDonald, R. J.; Smith, A. R.; Seacrist, M.; Moreland, J.; Shen, J.; Wahlich, R.; Weber, E. R. *J. Appl. Phys.* **2005**, *97*, 063503.
(24) David, A.; Porter, K. E. E. *Phase transformations in metals and alloys*; CRC Press: Boca Raton, FL, 1981.
(25) Tang, W.; Picraux, S. T.; Huang, J. Y.; Gusak, A. M.; Tu, K.-N.; Dayeh, S. A. *Nano Lett.* **2013**, *13*, 2748–2753.
(26) Kim, B. J.; Tersoff, J.; Kodambaka, S.; Reuter, M. C.; Stach, E. A.; Ross, F. M. *Science* **2008**, *322*, 1070–1073.
(27) Guliants, E. A.; Anderson, W. A.; Guo, L. P.; Guliants, V. V. *Thin Solid Films* **2001**, *385*, 74–80.
(28) Hayzelden, C.; Batstone, J. L. *J. Appl. Phys.* **1993**, *73*, 8279–8289.
(29) Xie, T.; Schmidt, V.; Pippel, E.; Senz, S.; Gösele, U. *Small* **2008**, *4*, 64–68.
(30) Hiraki, A.; Nicolet, M.-A.; Mayer, J. W. *Appl. Phys. Lett.* **1971**, *18*, 178–181.

(31) Dheurle, F.; Petersson, S.; Stolt, L.; Strizker, B. *J. Appl. Phys.* **1982**, *53*, 5678−5681.
(32) Chou, Y.-C.; Wu, W.-W.; Chen, L.-J.; Tu, K.-N. *Nano Lett.* **2009**, *9*, 2337−2342.
(33) Sutter, E.; Sutter, P. *Nano Lett.* **2008**, *8*, 411−414.
(34) Nadkarni, G. D.; Garoff, S. *Europhys. Lett.* **1992**, *20*, 523.
(35) Tu, Y.; Tersoff, J. *Phys. Rev. Lett.* **2000**, *84*, 4393−4396.
(36) Satpati, B.; Satyam, P. V.; Som, T.; Dev, B. N. *J. Appl. Phys.* **2004**, *96*, 5212−5216.
(37) Mangelinck, D.; Gas, P.; Grob, A.; Pichaud, B.; Thomas, O. *J. Appl. Phys.* **1996**, *79*, 4078−4086.